
New Trends in Physical Science Research
Vol. 1
B P International

Chapter 1
Print ISBN: 978-93-5547-615-9, eBook ISBN: 978-93-5547-616-6

Probe, Optical Emission and Quartz Crystal Microbalance Diagnostics in Hollow Cathode Magnetron

I. I. Usatov [a], N. P. Poluektov [a*], Yu P. Tsar'gorodsev [a], A. G. Evstigneev [a] and I. A. Kamyschov [a]

DOI: 10.9734/bpi/ntpsr/v1/15681D

ABSTRACT

The purpose of this paper is to describe the characterization of an ionized physical vapor deposition (IPVD) by means of hollow cathode magnetron. Measurements with the Langmuir probe, optical emission spectroscopy, and grid quartz crystal microbalance were used to investigate a mechanism for the production of excited argon and copper atoms and ions. The kinetic processes of excitation were considered, and the main processes were ascertained using measurement results. The pressure range was 0.5 - 10 mTorr with 1- 5 kW discharge power. Plasma parameters like electron densities and temperatures, electron energy distribution functions, plasma space and floating potentials as a function of position, pressure, and power in the growth chamber were calculated. The plasma density is up to 10^{12} cm^{-3} at 20 cm from the magnetron for 10 mTorr. Using a grid quartz crystal microbalance, the ionized copper flux fraction was measured as a function of the gas pressure, discharge power, and distance from the target. At gas pressures of higher than 15 mTorr, the degree of ionization at a distance of 31 cm exceeds 50%.

Keywords: Hollow cathode magnetron; ionized physical vapor deposition.

1. INTRODUCTION

The hollow cathode magnetron (HCM) is a plasma source for films deposition using of atoms and ions of metal. The high density plasma (more than 10^{12} cm^{-3} at pressure a few millitorrs) formed in a large (10^3 $cm^{3)}$ volume, as well as the low (10 - 50 eV) and easily changeable energy of the ions arriving at the substrate, are all features of this discharge. The main difference between this technique and conventional approaches is that a large proportion of the sputtered material is ionised, whereas in traditional magnetron sputtering, the sputtered species are almost entirely neutral [1-3].The ionized physical vapor deposition (IPVD) method is increasingly used to deposit diffusion barriers and copper seed layers materials into high-aspect ratio vias and trenches for microelectronics fabrication [1-4]. Ionized metal plasmas have been also used to produced nanosize interlayers and graded structures by intermixing of condensing ions and substrate. Metal plasmas are often used in deposition of nanosized compound multilayers that can undergo phase changes at elevated temperatures [5,6]. Film deposition in this discharge is accompanied by the streams of low-energy ions that allow to receive a film with unique properties. Several techniques have been developed for obtaining an ionized growth flux; the plasma may be generated, for example, by inductively coupled radio-frequency (rf) power [4-6] or by electron cyclotron resonance [7] and by high-power impulse magnetron systems (HiPIMS) [8-10]. HCM uses a single dc power supply to both sputter and ionize the target material unlike other IPVD tools which use secondary inductively coupled or ECR plasma sources for ionization of sputtered atoms. The quality of the deposited films depends on the quantity and energy of the particle flux and substrate temperature. In the HCM these values differ greatly from those in the convectional magnetron. In a conventional magnetron main contribution to the particle

[a] Bauman Moscow State Technical University, Mytishchi Branch, 141005, Mytischi-5, Moscow Region, Russia.
**Corresponding author: E-mail: poluekt@mgul.ac.ru;*

flux on the substrate is made by atoms of the target and buffer gas. In HCM main contribution is produced by ions of the buffer gas and metal. Such ion assistance allows the deposition of high quality films on complex shaped substrates. This type of discharge has received insufficient study, as can be judged from the relatively small number of publications on this subject.

The purpose of this paper is to study the mechanism for the production of excited argon and copper atoms and ions as well as the ionized copper flux fraction. For this the spatial distribution of plasma parameters in hollow cathode magnetron were studied using probe, optical emission spectroscopy and grid quartz crystal microbalance diagnostics.

2. EXPERIMENTAL APPARATUS

Fig. 1 presents our experimental set-up. The cathode consists of a cup-shaped Cu target (8 cm i.d. and 7 cm long) from which plasma diffuses into a reactor (35 cm diameter, 55 cm length). The chamber was pumped to base pressure $5 \cdot 10^{-6}$ Torr using a turbomolecular pump. Argon is used as the buffer gas.

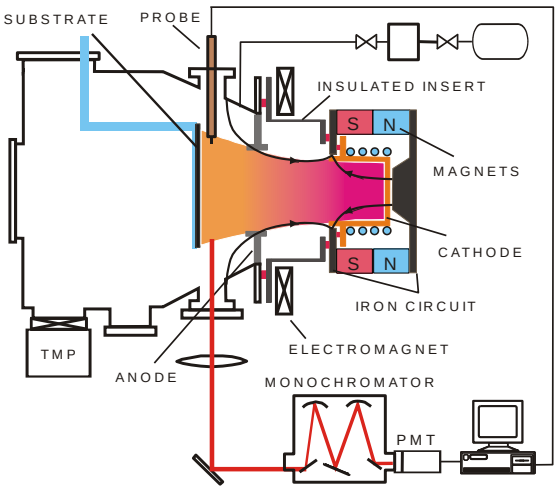

Fig. 1. Schema of the experimental set-up

Pressure was within range of 0.5 - 10 mTorr. Gas flow is provided by a gas flow controller. The HCM is powered with inverter source up to 12 kW (20 A, 600 V). The magnetic field with maximum of 800 Gs is produced by twelve columns of Nd-Fe-B magnets 18 x 20 x 120 mm^3 in size surrounded the target with ring iron flanges on the end. The downstream of the HCM is located the electromagnet that creates a magnetic field of opposite direction to the field of the permanent magnets. As a result, magnetic field is directed along a sidewall surface of the magnetron and has a cusp at the mouth of the cathode. Magnetic field captures secondary electrons emitted from the cathode, which produce an ionization of the buffer gas and sputtering atoms of the target. Crossed ExB fields cause electron drift in an azimuthal direction, in result inside the hollow cathode plasma of high density (> 10^{13} cm^{-3}) is created. The target utilization in such cathode is higher than in the magnetron with flat cathode. Fig. 2 shows the change in the thickness of the cathode measured along its length. The zone of erosion occupies almost all cylindrical part.

Outside of the hollow cathode there is the region where the magnetic field strength is equal to zero. This area separates the plasma that exists in the hollow cathode from plasma which flows toward the substrate. Those electrons and ions which have initial axial velocities are capable to leave the hollow cathode and to be distributed to a substrate. The plasma stream has a core with diameter of about 4 cm at a distance of 20 cm from a magnetron. For expansion of plasma stream and creation of more homogeneous radial distribution is used the electromagnet that creates a diverging magnetic field outside the magnetic null region. The electrically insulated anode is located between the cathode and plasma chamber to create a potential difference with respect to HCM.

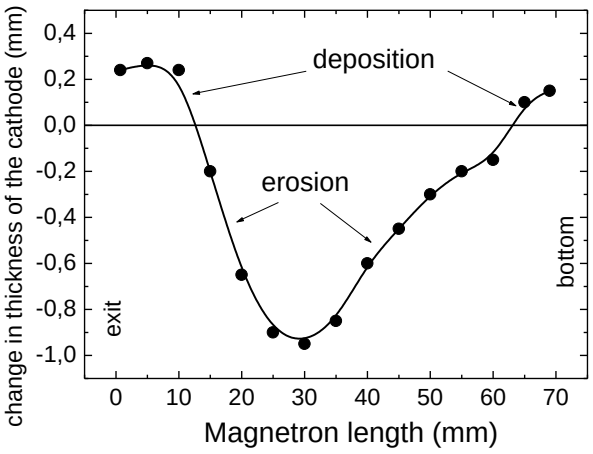

Fig. 2. **Structures of the target erosion**

The electron temperature, electron energy distribution function, ion density, floating and plasma potentials were determined from probe measurements. The probe tip was made of a tungsten wire 0.35 mm in diameter and 5 mm long. The probe was located at a distance of 20 cm from exit of a magnetron and 3 cm before a substrate. The substrate was isolated from chamber wall. It should be noted that probe measurements in this plasma are not a simple task due to metal deposition on the probe. Discharge power is kWatts and metal flux is large. In the article [9] his issue is considered in details.

Therefore, we created a system for rapid record of the probe characteristics. The *I*–*V* characteristics were recorded with the help PCI card National Instruments NI6221 with a 16 bit ADC, a 16 bit DAC and multiplexer. The ADC and DAC were connected to a probe via isolated modules. The DAC voltage was increased by self-made powerful voltage amplifier (with an output voltage range from –80 to +80 V at an output current of up to 800 mA and a voltage rise time of up to 10 V/s). The *I-V* characteristic includes up to 640 pairs. In dense plasma the number of points is less (420-450) as the voltage range is limited to +15-+20 V due to large electron saturation current. To improve the accuracy of measurements, each pair of current-voltage points is obtained by averaging of the set of 10 data points. The time required to obtain one *I-V* curve is about 2 s. The LabView software is used for the measurement program.

The program of data processing is written in MatLAB language. At first the data smoothing by B - splines is made and then the plasma potential and electron energy distribution function (EEDF) are calculated from the second derivative. The need for this procedure is due to the fact that experimental data have large noises caused by fluctuations of plasma. In the plasma of our discharge the ratio of probe radius to Debye radius is about of 10, therefore analytical Langmuir theory is not applied for the probe analysis. For calculation of electron density is used the parametrization of the Laframboise theory [11]. The algorithm used in the program is the development of the method described in [12]. The electron temperature is defined as average temperature:

$$T_e = \frac{2}{3k_B} \frac{\int_0^\infty E f(E)\,dE}{\int_0^\infty f(E)\,dE}, \qquad (1)$$

where E, k_B, $f(E)$ are the energy of the electrons, the Boltzmann constant and the energy distribution function of electrons respectively.

Plasma emission was monitored through windows located at 20 cm downstream the magnetron in the conical part of the chamber. To prevent quartz windows from metal deposition two 5 cm tubes with 1.5 cm diaphragm are located inside the chamber, providing between them 15 cm length trough plasma.

Spectra of plasma emission were measured by a grating monochromator (1200 lines mm^{-1}, inverse dispersion 2.4 nm/mm) equipped with a photomultiplier tube (PMT).

The ionization fraction of metal flux is an important parameter, on which the quality of the obtained films largely depends. The ionization fraction of metal flux γ is defined as the ratio of the ion flux to the total flux of metal atoms and ions [13].

$$\gamma = \frac{\Gamma_{Cu+}}{\Gamma_{Cu^+ + Cu}}, \tag{2}$$

Where

$$\Gamma_{Cu} = 0.25\, n_{Cu} \sqrt{\frac{8 k_Б T_{Cu}}{\pi M_{Cu}}} \tag{3}$$

$$\Gamma_{Cu^+} = 0.6 n_{Cu^+} \sqrt{\frac{k_B T_e}{M_{Cu}}} \tag{4}$$

are the fluxes of copper atoms and ions, respectively. Here, M_{Cu} is the mass of a copper atom; and T_{Cu} and T_e are the temperatures of copper atoms and electrons, respectively.

The degree of ionization of the flow was measured using a grid quartz crystal microbalance (g-QCM) - an industrial Inficon sensor in front of which two grids were installed. The QCM and the first grid were insulated from the chamber and were under the plasma floating potential.

The grids are made of 50-μm-thick stainless-steel foil [14]. The square mesh size is 70 μm, and the wire width is 30 μm, the grid transparency being Tg = 50%. The grids are insulated from one another by mica rings with a thickness of 0.8 mm, an inner diameter of 18 mm, and an outer diameter of 22 mm. The first grid is under the floating potential and retards a considerable fraction of the electron flow. The second grid is at a positive (with respect to the plasma) potential and retards ions. The grid efficiently retards ions if the distance between the wires does not exceed two Debye radii λ_{De}. This condition can be expressed as follow:

$$L_{redard} = 2\lambda_{De} = 2 \cdot 740 \sqrt{\frac{T_e}{N_e}} \tag{5}$$

where T_e is in eV and the electron density N_e is in cm^{-3}. For T_e = 2.5 eV and a cell size of 70 μm, the maximum plasma density at which the plasma flow is retarded by the grid is $5 \cdot 10^{11}$ cm^{-3}.

The results of measurements are also affected by the geometric factor *G*, which depends on the ratio between the height and diameter of the sensor (the aspect ratio) [2]. In front of the quartz crystal, round grids are installed; hence, the crystal is located at the bottom of a well. A fraction of neutral atoms having an isotropic velocity distribution do not reach the well bottom, i.e., the flux of atoms onto the surface of the first grid, Γ_{Cu_plasma}, differs from that onto the well bottom, $\Gamma_{Cu\_crystal}$. As a result, the value of γ turns out to be overestimated. To take this effect into account, the geometric factor G ≤ 1 is introduced. In our case, the diameter of the grid is 18 mm and the distance from the grid to the crystal

sensor is 4 mm, i.e., the well is not deep and the aspect ratio is as low as 0.22. In addition, the sensor diameter is 8 mm and the distribution of neutral atoms differs from isotropic, because metal particles are sputtered from the side surfaces of the cylindrical target. For this reason, we assumed that G = 1. Since our measurements were performed at gas pressures of lower than 20 mTorr, the influence of particle collisions inside the sensor could be ignored.

3. RESULTS AND DISCUSSION

3.1 Probe Diagnostics

Fig. 3 shows current – voltage (I-V) characteristics of the magnetron discharge for various pressure. The (I-V) characteristics are well approximated by the relationship $I = kV^n$ with n = 7-10. With increasing pressure, the discharge voltage decreases for the same currents, it is connected to growth of plasma density. The probability of ionization is proportional to neutral particles density and this effect is greater than the reduction of electron temperature, which results in opposite effect. Figure 4 shows an effect of a magnetic field of an electromagnet on the radial plasma characteristics. The increase of a magnetic field of the electromagnet results in growth of uniformity of a stream and to a decrease of plasma density. At discharge power of 3 kW and pressure of 10 mTorr plasma density on an axis decreases from $7.2 \cdot 10^{11}$ cm^{-3}, when electromagnet is turned off, to $3 \cdot 10^{11}$ cm^{-3} when electromagnet current is equal to 1.2 A. Let's note also, that energy of ions on the isolated substrate equal $e\,(V_s - V_f)$ does not exceed 20 eV.

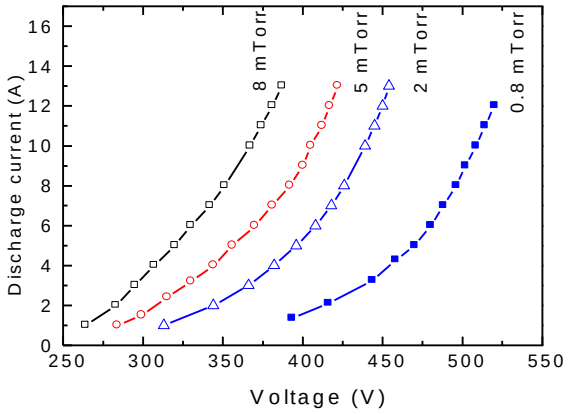

Fig. 3. Current-voltage characteristics of the HCM for various pressures.

Mean electron temperature, floating and plasma potentials decrease when electromagnet current increases. Probably, it occurs owing to growth of the electron losses on excitation and ionization of atoms at increase of cross section of a stream. Nevertheless, the higher values of electron density and temperature on this distance allow effectively ionize the sputtered metal atoms for a way from the target to the substrate. It should be noted , that plasma density inside of the cathode changes very little, as I-V characteristics of the discharge depend poorly on a current of an electromagnet. Thus, change of plasma density occurs outside of the cathode where magnetized electrons move along divergent magnetic field lines of the electromagnet on lateral walls of the chamber and by ambipolar diffusion pull behind itself ions.

Effect of the magnetron power on plasma parameters on the discharge axis is shown in Fig. 5. The plasma density (Fig. 5(a)) grows almost linearly with a power up to a level of 2 kW, then slope decreases. Such behavior can be explained by a decrease of the local argon density due to heating by sputtered copper atoms. Plasma and floating potentials, average electron temperature depend poorly on a power (Fig. 5b). Note the mean electron temperature increases with a magnetron power. This fact is not evident for high power

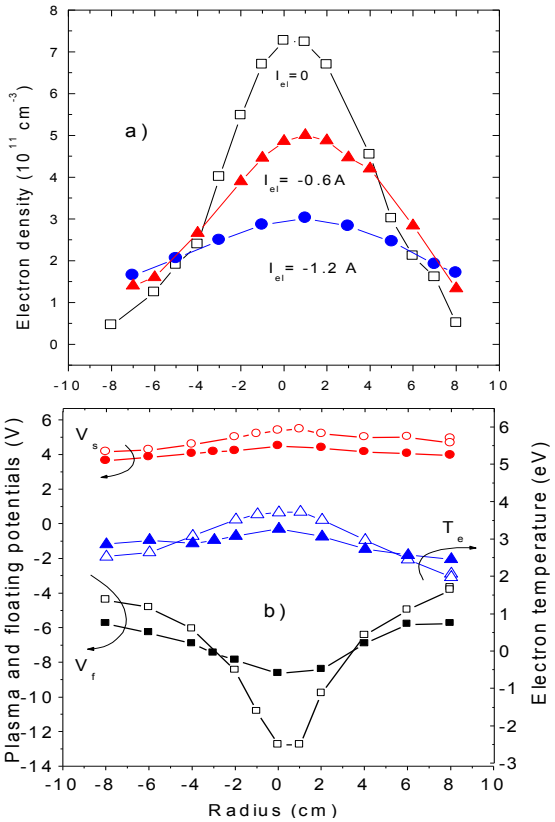

Fig. 4. Radial profiles of: a) the electron density N_e ; b) electron temperature T_e, floating V_f and plasma V_s potentials. 20 cm from the target. p = 10 mTorr, 50 sccm, W = 3 kWatt. Open symbols - I_{el} = 0 A, solid symbols - I_{el} = -0.6 A

IPVD discharges. In [3-5,9,10] the electron temperature decreases for high magnetron current due to very large number of sputtered metal atoms. The energy thresholds for electron impact excitation and ionization of metal atoms (<8 eV) are much lower than those for argon. As a result, metal atoms act as a energy absorbers in the discharge, preventing electrons from reaching energies as high as in pure argon discharge. Different results can be explained as follow. In [9] discharge pressure was in the range of 30-50 mTorr and mean electron temperature has a maximum of 1.5 eV. Consequently, the number of electrons with energy greater than 8 eV was much less than at pressure 5-10 mTorr with the electron temperature 3-4 eV. So, the lack of these electrons reduces the mean electron temperature when the number of metal atoms strongly increases.

Fig. 6 shows the plasma potential V_S, floating potential V_f, and electron temperature as function of a distance from the magnetron at pressures of 2 and 5 mTorr. Near the target plasma density rises with growth of a pressure. Electrons lose its energy be collisions and at a distance of 30 cm electron density for 5 mTorr becomes less than the one for 2 mTorr. Nevertheless, at that distance plasma density exceeds 10^{11}cm^{-3}.

Fig. 7 presents on the logarithmic scale the electron energy probability function (EEPF) obtained by dividing the electron energy distribution function (EEDF) by $\sqrt{E}$. This function is convenient because for a Maxwellian distribution, its logarithm depends linearly on the electron energy [15]. As can be seen from the EEPF plots the energy distributions roughly agree with Maxwellian up to 20 eV. The high plasma density provides a strong Maxwelliziing effect due to electron-electron collisions. Beginning from 20 eV there is a depletion of EEDF due to the inelastic (excitation and ionization) electron collisions with argon atoms. A number of high energy electrons decreases with an increase of distance from cathode. Nevertheless, there are many electrons which are able to ionize the copper atoms (the Cu ionization energy is equal to 7.72 eV).

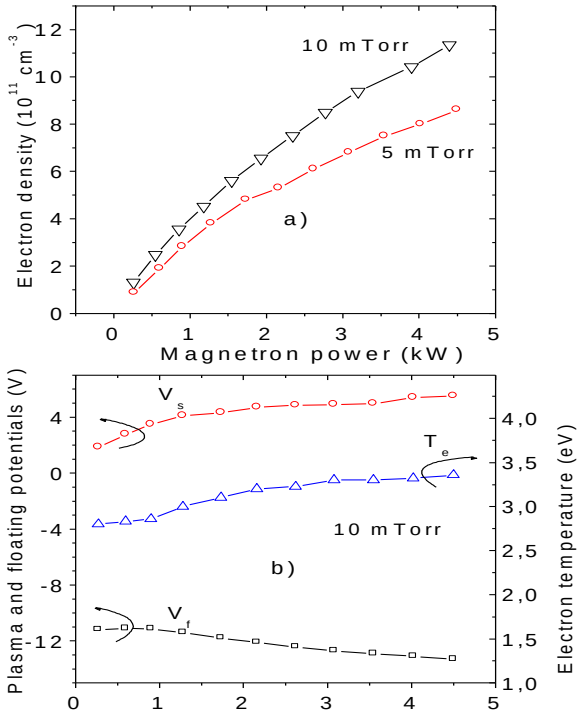

Fig. 5. a) Electron density; b) plasma potential V_s, floating potential V_f, and mean electron temperature T_e; as function of the magnetron power. I_{el} = -0.6 A. 20 cm from the target

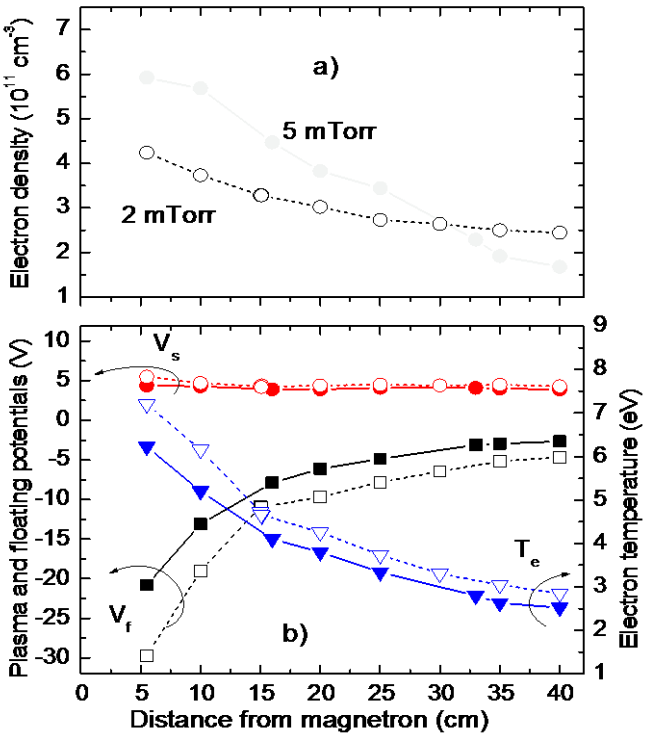

Fig. 6. Axial distribution from the target exit of a) electron density N_e; b) electron temperature T_e, plasma V_s and floating V_f potentials
Solid lines - p= 5 mTorr, I = 4 A, U = 323 V
Dot lines - p= 2 mTorr, I = 4 A, U = 370 V.
$I_{el.-magn}$ = 0 A

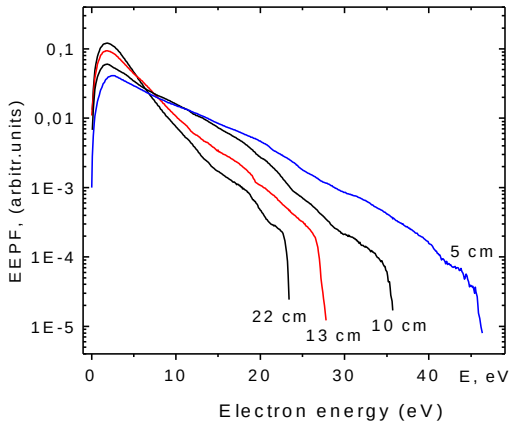

Fig. 7. Normalized electron energy distribution function on the discharge axis. p = 5 mTorr, W =1.3 kWatt

3.2 Optical Emission Spectroscopy

The optical emission spectroscopy of Ar/Cu plasma was performed as a function of a power and pressure. A typical emission spectrum of wavelength between 210 and 830 nm from Cu/Ar plasma is shown in Fig. 8 (the intensities of the resonance lines Cu324.7 and Cu327.4 nm are reduced by 5 times).

The spectral line intensity $I((\nu_{ij})$ in optically thin plasma is related to the density atoms in the excited state $[X^*]$ by [16]:

$$I(\nu_{ij}) = c(\nu_{ij})h\nu[X^*]A_{ij} = K^{\nu}[X^*], \tag{6}$$

where K^{ν} is a constant specific to each emitted line frequency ν, $c(\nu_{ij})$ is the spectral response of the monochromator and detector, h - Plank's constant. $\Sigma_j A_{ij}$ represents the sum of all radiative deexcitation frequencies from upper level i to lower level j. At higher electron density (>10^{11} cm^{-3}) the electron impact excitation and ionization dominate the Penning mechanism [3,4]. When the concentration of electrons is high collisions decrease the metastable lifetime and therefore this mechanism can be neglected.

Then the density of a radiative upper state only populated by electronic collisions depends on the electronic density n_e:

$$[X^*] = \frac{[X]n_e C^i}{\Sigma_j A_{ij} + n_e C_i}, \tag{7}$$

here C^i and C_i are the production and destruction rates of upper state and $[X]$ density of lower state. For neutral and ionic copper and argon, the radiative loss frequency $\Sigma_j A_{ij}$ is about 10^7 – 10^8 s^{-1}. According to [15], the loss frequency first excited state of Ar and Cu by electronic collision is one order less for $n_e < 10^{12}$ cm^{-3}. We therefore assumed that the losses by spontaneous photon emission were dominant process compared with electronic impact loss.
Then Equation (6) is written as:

$$I(\nu_{ij}) = K^{\nu}\frac{n_e[X]C^i}{\Sigma_j A_{ij}} = K_{ij}n_e[X]C^i, \tag{8}$$

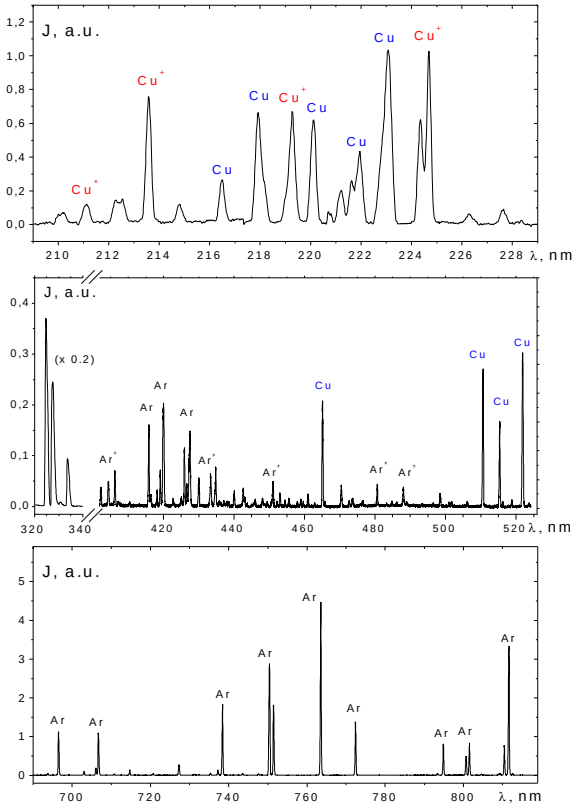

Fig. 8. An optical emission spectrum from Ar/Cu plasma at wavelength between 210 and 830 nm. p = 5 mTorr, $I_{el\text{-}mag}$ = - 0.4 A, W = 3.36 Kw

The rate coefficient for electron excitation C^i depends on the *EEDF* and the spectral line intensity is:

$$I(\nu_{ij}) = K_{ij} n_e [X] \int_{E_t}^{\infty} \sigma v f(E) dE = K_{ij} n_e [X] k(T_e), \tag{9}$$

where σ is the velocity-dependent cross section for electron impact excitation, f (E) is the electron energy distribution function, v is the electron velocity, E and E_t represent the electron energy and the excitation threshold energy respectively. For a Maxwellian distribution of electron energies, the integral in Eq. (9) is a function of electron temperature represented by an electron temperature dependent rate constant $k(T_e)$. There are two processes, which have the opposite effect on the emission intensity when magnetron power rises. We suppose that rarefaction by buffer gas heating compensates a little growth in electron temperature with increasing discharge power, as probe measurements show that the EEDF depends weakly on a power. Then the emission intensities from both Cu neutrals and Cu^+ ions are proportional to the density of the species. The ratio of the emission intensities from Cu neutral and Cu ion lines at a constant argon pressure will be proportional to the degree of Cu ionization.

Fig. 9 compares the emitted intensities for Cu neutral (216 nm) and Cu^+ ion (213.6 nm) lines versus discharge power for argon pressure 10 mTorr. Since these lines are close to each other, the photomultiplier sensitivity is equal for them. The emitted intensity from Cu atom exceeds intensity from Cu^+ for power less than 1 kW. With increasing power, the situation is reversed and at discharge power of 3.5 kW the ion emission intensity is about three times higher atom intensity.

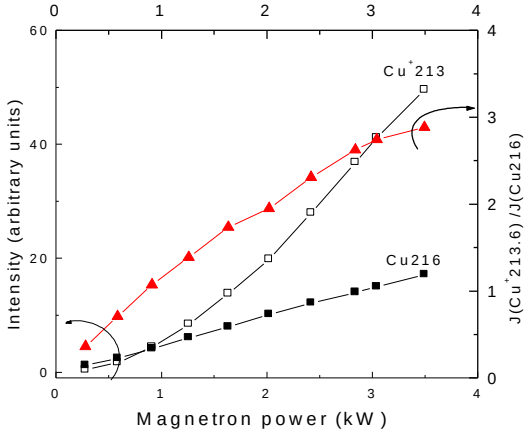

Fig. 9. The optical emission intensities from Cu ion lines (213.6 nm) and Cu neutral (216.5 nm) at 10 mTorr vs discharge power

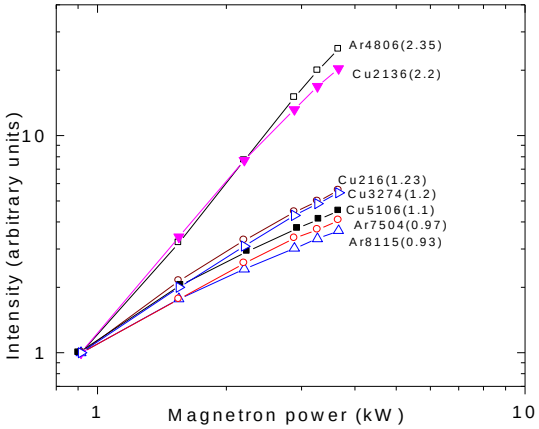

Fig. 10. Normalized intensities of Ar and Cu spectral lines as function of a magnetron power, I_{el} =-0.5 A, 10 mTorr

Thus, an increase of electron density with power rise causes effective ionization of the sputtered Cu atoms.

Fig. 10 shows the normalized intensities of Ar and Cu spectral lines as function of a magnetron power (intensity at W = 0.9 kW is accepted for 1) in logarithmic coordinates (numbers within parenthesis show the degree of dependence). These data do not depend on the spectral sensitivity of PMT. It is seen that intensities of radiation of argon and copper atoms increase nearly linear with power. The intensities of argon and copper ions are proportional to about square of the magnetron power. As already noted, the EEDF depends weakly on a power. Therefore, dependence of intensity emission is determined mainly by the electron density.

For simplicity, we apply a rather rough assumption that the influence of metastable states is small. Then the following mechanisms are considered for the creation of excited states of argon ions:

$$e + Ar \rightarrow Ar^{+*} + e + e, \qquad k^{+*}_{e,Ar}, \tag{10}$$

$$e + Ar^{+} \rightarrow Ar^{+*} + e, \qquad k^{+*}_{e,Ar^{+}}, \tag{11}$$

where $k^{+*}_{e,Ar}$, k^{+*}_{e,Ar^+} are the rate coefficients. The excited argon ions density is expressed by:

$$[Ar^{+*}]_{atom} = n_e[Ar]\left(\frac{k^{+*}_{e,Ar}}{\Sigma_j A^{Ar^{+*}}_{ij}}\right) = n_e[Ar]C^{atom}_{+*}, \tag{12}$$

if the electron collides with the atom (see(10)), and

$$[Ar^{+*}]_{ion} = n_e[Ar^+]\left(\frac{k^{+*}_{e,Ar^+}}{\Sigma_j A^{Ar^{+*}}_{ij}}\right) = n_e[Ar^+]C^{ion}_{+*}, \tag{13}$$

if the electron collides with the ion (see 11). Here *[Ar]*, *[Ar^+]* are atom and ion densities in the ground state respectively.

The main creation mechanism for argon ions in the ground state is an electronic collision, with the rate coefficient $k^{+}_{e,Ar}$:

$$e + Ar \rightarrow Ar^+ + e + e, \qquad k^{+}_{e,Ar} \tag{14}$$

Density of non-radiative species are defined by the losses in electronic collisions and diffusion to the reactor walls. Then in stationary state the density of argon ions in the ground state is given by [17]:

$$[Ar^+] = n_e[Ar]\left(\frac{k^{+}_{e,Ar}}{\nu^{D}_{Ar^+} + n_e k^{+*}_{e,+}}\right), \tag{15}$$

where $\nu^{D}_{Ar^+}$ and $n_e k^{+*}_{e,+}$ are the loss frequencies of the argon ion by diffusion and by electron collisions respectively. If the diffusion term is much less than the collision term, then the following expression is obtained from (15):

$$[Ar^+]_{coll} = \frac{[Ar]k^{+}_{e,Ar}}{k^{+*}_{e,+}} = [Ar]C^{coll}_{+} \tag{16}$$

Otherwise we have:

$$[Ar^+]_{diff} = \frac{n_e[Ar]k^{+}_{e,Ar}}{\nu^{D}_{Ar^+}} = n_e[Ar]C^{diff}_{+}, \tag{17}$$

where the constants C^{coll}_{+} and C^{diff}_{+} are defined as the ratio between the creation coefficient and the loss coefficient. At constant pressure they are assumed do not depend on discharge power.
Using (6) the emitted intensity of the Ar ion is

$$I(Ar^{+*}) = K^{Ar^+}_{ij} n_e[Ar]C^{atom}_{+*}, \tag{18}$$

if argon ion excited from the argon neutral (see (12). When argon ion excited from the ion ground state and minor diffusion (see (13) and (16)), the intensity can be written:

$$I(Ar^{+*}) = K^{\nu}[Ar^{+*}]_{ion} = K^{\nu} n_e [Ar^{+}]_{coll} C_{+*}^{ion} = \\ = K^{\nu} n_e C_{+*}^{ion} [Ar] C_{+}^{coll} \quad (19)$$

If argon ion excited from the ion ground state and dominant diffusion (see (13 and 17)) we have:

$$I(Ar^{+*}) = K^{\nu}[Ar^{+*}]_{ion} = K^{\nu} n_e [Ar^{+}]_{diff} C_{+*}^{ion} = \\ = K^{\nu} n_e C_{+*}^{ion} n_e [Ar] C_{+}^{coll} \quad (20)$$

It is seen from the previous expressions, that the emission intensity is related to the electronic density, which is about linearly proportional to the magnetron power.

The intensities of argon ions are proportional to about square of the magnetron power as it follows from Fig. 9. This implies that the main losses for argon ions are by diffusion at 20 cm according to expression (20).

Similar equations can be obtained for copper atom and ion lines. The copper atom density in the ground state at the steady state is given by:

$$[Cu] = \frac{\gamma_{Cu}[Ar^{+}]}{\nu_{Cu}^{D} + n_e k_{e,Cu}^{+}}, \quad (21)$$

where γ_{Cu} is the sputtering coefficient and $k_{e,Cu}^{+}$ is the destructive rate by ionization in the following reaction:

$$e + Cu \rightarrow Cu^{+} + e + e \quad (22)$$

If copper excited states are supposed to be created mainly by the electron impact on the copper ground state:

$$e + Cu \rightarrow Cu^{*} + e, \quad (23)$$

then the line intensity can be expressed versus electronic density as:

$$I(Cu^{*}) \propto n_e [Cu] \propto \\ \propto \frac{n_e \gamma_{Cu}[Ar^{+}]_{diff}}{\nu_{Cu}^{D} + n_e k_{e,Cu}^{+}} \propto \frac{n_e^2 \gamma_{Cu}[Ar]}{\nu_{Cu}^{D} + n_e k_{e,Cu}^{+}} \quad (24)$$

Here we used Eqs.(13) and (17). If diffusion term ν_{Cu}^{D} is much less than collision term $n_e k_{e,Cu}^{+}$,

$$\nu_{Cu}^{D} << n_e k_{e,Cu}^{+} \quad (25)$$

we obtain:

$$I(Cu^{*}) \propto n_e \quad (26)$$

Fig. 10 shows that emission intensity of copper atoms increases linearly with a slope 1. Thus, the proposed kinetic scheme with the expressions (13) and (17) explains the observed behavior of Cu line

intensities, indicating that copper atoms were lost due to the ionization by electron collisions at a distance of 20 cm from magnetron.

Another argument in favor of this conclusion is the results of experiments on the absorption of resonance lines of copper. Fig. 11 shows the absorption coefficient A of the resonance Cu line 324.7 nm, obtained at a distance of 20 cm vs magnetron power. $A = 1 - \frac{I_{L+P} - I_P}{I_L}$, where I_L is the light intensity of the lamp with hollow cathode, I_P *i*s intensity of Cu atoms in plasma, when lamp off and I_{L+P} is the intensity, measured with lamp and plasma on. When current of electromagnet I_{el} = -1.25 A plasma density at this distance is low (see Fig.4) and the ionization of Cu atoms is also small. Density of sputtered Cu atoms increases with growing power and coefficient A grows. When I_{el} = - 0.6 A plasma density downstream the magnetron is great and increases with magnetron power. The ionization of Cu atoms rises also, density of Cu atoms decreases and coefficient A falls. Recall that value of the sputtered Cu atoms inside of the cathode is about the same in both cases. These measurements confirm our conclusion that the ionization of Cu atoms is dominant loss term at a distance of 20 cm from magnetron. Detailed description of these measurements is beyond scope of this article.

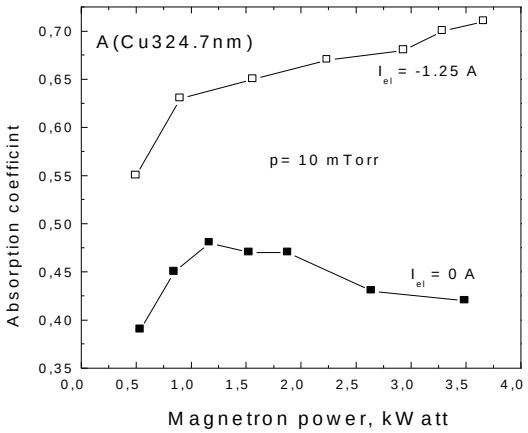

Fig. 11. Absorption coefficient A of the Cu spectral line 324.7 nm as function of magnetron power

For the emission intensity of the copper ion we consider two-step mechanism:

$$Cu^+ + e \rightarrow Cu^{+*} + e, \tag{27}$$

where Cu^+ is produced by reaction:

$$Cu + e \rightarrow Cu^+ + e + e \tag{28}$$

Then

$$I(Cu^{+*}) \propto n_e[Cu^+] \tag{29}$$

The copper ion density in the ground state is given by analogy to (11):

$$[Cu^+] = n_e[Cu]\left(\frac{k^+_{e,Cu}}{\nu^D_{Cu^+} + n_e k^+_{e,Cu^+}}\right) \tag{30}$$

Using condition (25), Eqs. (17), (21) and (30) it can be deduce:

$$I(Cu^{+*}) \propto n_e[Cu^+] \propto \frac{n_e^2[Cu]}{(\nu^D_{Cu^+} + n_e k^+_{e,Cu^+})} \propto$$
$$\propto \frac{\gamma_{Cu} n_e^2 [Ar^+]_{diff}}{(\nu^D_{Cu^+} + n_e k^+_{e,Cu^+})(\nu^D_{Cu} + n_e k^+_{e,Cu})} \propto \quad (31)$$
$$\propto \frac{\gamma_{Cu} n_e^3[Ar]}{(\nu^D_{Cu^+} + n_e k^+_{e,Cu^+}) n_e k^+_{e,Cu}} \propto$$
$$\propto \frac{n_e^2[Ar]}{(\nu^D_{Cu^+} + n_e k^+_{e,Cu^+}) k^+_{e,Cu}}$$

The copper ion diffusion term $\nu^D_{Cu^+}$ is much more than total destructive (including double ionization) term $n_e k^+_{e,Cu^+}$. So that,

$$I(Cu^{+*}) \propto n_e^2 \quad (32)$$

Thus, from the change in the intensity of the Cu and Cu^+ spectral lines depending on the power of the magnetron, we can conclude that the dominant losses are electron ionization for copper atoms and diffusion for copper ions.

In our model we neglect the influence of metastable states of Cu and Ar atoms. Our measurements of the absorption coefficient of the line Cu510.6 nm shown that density of the metastable level $^2D_{5/2}$ is of an order less than density of the ground level. From the absorption coefficient of Ar696.5 and Ar811.5 nm lines we calculated density of metastable Ar level s_5 (Pashen notation). The Ar metastable state density were found in the range of 10^{10} – 10^{11} cm^{-3}. Note that these data were obtained at a distance 20 cm from the target. Data on metastable Ar atoms are in good agreement with the results obtained in a high-density plasma discharge [18-20]. We also did not account for Penning ionization of Cu and Ar atoms. Due to these factors, the experimental intensities of Ar^+, Cu and Cu^+ increase faster. However, these differences are small, indicating that these processes make a small contribution to ionization process.

3.3 Grid Quartz Crystal Microbalance Diagnostics

The g-QCM makes it possible to quantitatively measure the fluxes of ions and atoms onto the substrate.

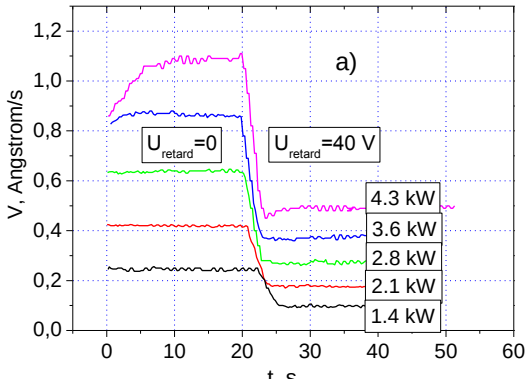

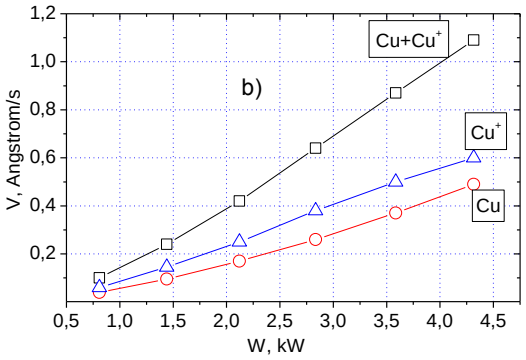

Fig. 12. (a) Signals from the grid QCM and (b) deposition rates of copper atoms and ions, as well as their total deposition rate, at a distance of 31 cm from the target and pressure of p = 15 mTorr as functions of the discharge power

Fig. 12a shows signals from the grid QCM recorded at different discharge powers. It is seen that the deposition rate (in this case, of copper atoms only) decreases abruptly after the retarding voltage U_{red} is switched on at t = 20 s. Fig. 12b shows the deposition rates of copper atoms and ions, as well as the total deposition rate as functions of the discharge power at a distance of 31 cm and gas pressure of 15 mTorr. The deposition rates are seen to increase with increasing power, the contribution of copper ions being larger than that of atoms.

Fig. 13 shows the ionization fraction of the sputtered copper flux γ as a function of the discharge power at different gas pressures and distances from the target. It is seen that γ increases with increasing gas pressure and distance from the target cathode. At pressures of 5 and 20 mTorr, the ionization fraction of the Cu flux increases from 0.2 to 0.4 at a distance of 19 cm and from 0.27 to 0.6 at a distance of 31 cm. As the distance increases, γ increases by 10% at pressures of 5 and 10 mTorr and by 20% at 15 and 20 mTorr. The ionization path length is described by the formula [15]:

$$\lambda_i = v_{Cu} / K_{ij} n_e. \qquad (33)$$

Here, v_{Cu} is the velocity of sputtered metal atoms, K_{ij} is the ionization rate constant (see formula (9)). The quantity K_{ij} is well fitted by the formula [15]:

$$K_{ij} \approx K_{i0} \exp(-E_i / T_e), \qquad (34)$$

where $K_{i0} = 5.62 \cdot 10^{-8}$ cm^{-3}/s for copper atoms [21], E_i is the ionization energy.

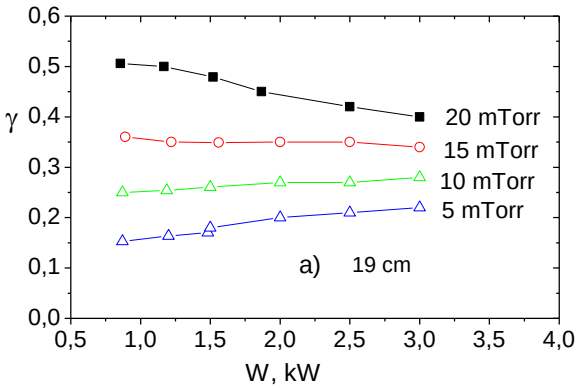

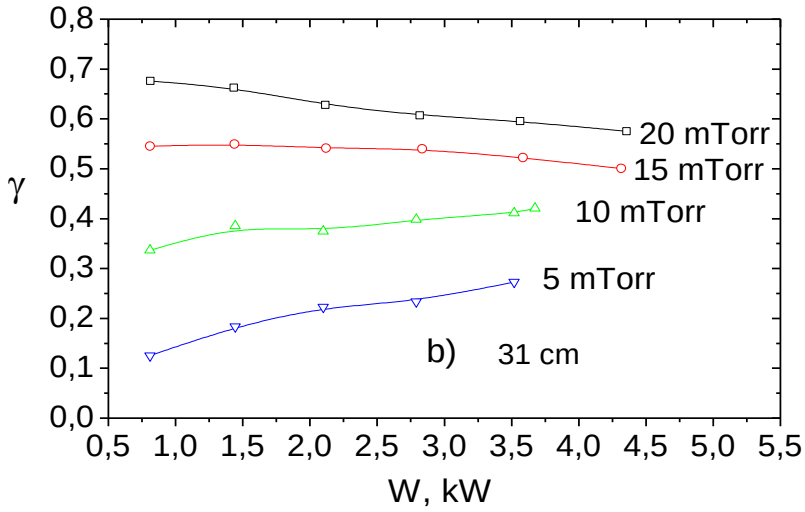

Fig. 13. Ionization fraction of the copper flux as a function of the discharge power at Iel = 3.5 A, different gas pressures, and different distances from the target-cathode: (a) 19 and (b) 31 cm

Due to collisions with neutral gas atoms, copper atoms lose their energy (are thermalized), their velocity decreases, and the time during which they stay in the discharge (and, accordingly, the probability of their ionization) increases. We remind that the electron density at these distances exceeds 10^{11} cm^{-3} and there are a lot of electrons with energies higher than the ionization energy of copper.

Thus, from formulas (33) and (34), the observed dependence of the ionization probability on the power and pressure becomes quite clear.

The experiments have shown, that hollow cathode magnetron discharge allows to receive plasma density more than 10^{11} cm^{-3} at a distance in tens cm at pressure in some mTorr. The high plasma density created in the large volume, increases probability of ionization of the sprayed atoms of a target. The stream of ions of the target, controlled by an electric field near a substrate, enables to deposit a highly conformal film on structures of the complex form. The size, uniformity, a degree of ionization of a stream of plasma can be supervised by the appropriate choice of power, pressure, magnitude and configuration of a magnetic field.

4. CONCLUSION

Langmuir probe, optical emission spectroscopy and grid-QCM measurements were used to study of plasma characteristics and Cu ionization in HCM discharge. The pressure range is 1-10 mTorr with 1-5 kW discharge power. Variation in the plasma parameters such as electron densities and temperatures, electron energy distribution function, plasma space and floating potentials as a function of the position, pressure and power in the growth chamber were measured in detail. The optical emission spectroscopy at a distance of 20 cm from magnetron shows strong increase of the intensity ratio from Cu^+ ion and Cu neutral lines with the power. These measurements indicated large downstream ionization of sputtered copper atoms. From the intensity variation of argon and copper atoms and ions spectral lines with magnetron power, it is deduced that the main creation mechanism for argon and copper ions is an electronic collision from the ground state and the dominant loss terms are electron ionization for copper atoms and diffusion for the ions. Using a grid QCM crystal microbalance, the ionized copper flux fraction was measured as a function of the gas pressure, discharge power, and distance from the target. At gas pressures of higher than 15 mTorr, the degree of ionization at a distance of 31 cm exceeds 50%.

COMPETING INTERESTS

Authors have declared that no competing interests exist.

REFERENCES

1. Klawuhn E, D'Couto GC, Ashtiani KA, Rymer P, Biberger MA, Levy KB. Ionized physical-vapor deposition using a hollow-cathode magnetron source for advanced metallization. J. Vac. Sci. Technol. 2000;18A(4):1546-1549.
2. Wu L, Ko E, Dulkin A, Park KJ, Fields S, Leeser K, Meng L, Ruzic DN. Flux energy analysis of species in hollow cathode magnetron ionize physical vapor deposition of copper", Rev.Scient.Instrum. 2010;81(12):123502.
3. Meng L, Raju R, Flauta R, Shin H, Ruzic DN. In situ plasma diagnostics study of a commercial high-power hollow cathode magnetron deposition tool. J. Vac. Sci. Technol. 2010; 28A(1):112-118.
4. Hopwood J. Ionized physical vapor deposition of integrated circuit interconnects", Physics of Plasmas. 1998;5(5):1624-1631.
5. Ostrikov K, Mutphy AB. Plasma-aided nanofabrication: where is the cutting edge?. J. Phys. D: Appl. Phys. 2007;40:2223–2241.
6. Anders A. Metal plasmas for the fabrication of nanostructures. J. Phys. D: Appl. Phys. 2007; 40:2272–2284.
7. Gorbatkin SM, Rossnagel SM. Cu metallization using a permanent magnet ECR microwave plasma/sputtering hybrid system. J. Vac. Sci. Technol. 1996;14B(3):1853-1859.
8. Maca´k K, Kouznetsov V, Schneider J, Helmersson U, Petrov I. Ionized sputter deposition using an extremely high plasma density pulsed magnetron discharge. J. Vac. Sci. Technol. A. 2000; 18(4):1533-1537.
9. Gudmundsson JT, Brenning N, Lundin D, Helmersson U. High power impulse magnetron sputtering discharge. J. Vac.Sci. Technol. 2012;30A:030801.
10. Anders A. Tutorial: Reactive high power impulse magnetron sputtering (R-HiPIMS). J. Appl. Phys. 2017;121:171101.
11. Laframboise JG. Theory of spherical and cylindrical Langmuir probes in a collisionless Maxwellian plasma at rest. Report No 100 Toronto Institute for Aerospace Studies, University of Toronto; 1966.
12. Mausbach M. Parametrization of the Laframboise theory for cylindrical Langmuir probe analysis. J. Vac. Sci. Technol. 1997;15A(6):2923-2929.
13. Green KM, Hayden DB, Juliano DR, Ruzic DN. Determination of flux ionization fraction using a quartz crystal microbalance and a gridded energy analyzer in an ionized magnetron sputtering system. Rev. Sci. Instrum. 1997;68:4555-4560.
14. Yu P, Tsar'gorodtsev NP, Poluektov II, Usatov AG, Evstigneev I, Kamyschov A. Ionization Fraction of the Sputtered Metal Flux in a Hollow Cathode Magnetron. Plasma Physics Reports. 2014;40(9):754-758.
15. Lieberman MA, Lichtenberg AJ. In Principles of Plasma Discharges and Materials Processing. Wiley, New York; 1994.
16. Mc Whirter RW. In: R. W. McWhirter. Spectral intensities. Ed. Plasma Diagnostic Techniques, RH. Huddlestone and S. L. Leonard, Academic, New York. 1965;165-217.
17. Nouvellon C, Konstantinidis S, Dauchot, JP, Wautelet M, Jouan PY, Ricard A, Hecq M. Emission spectrometry diagnostic of sputtered titanium in magnetron amplified discharge. J. Appl. Phys. 2002;92(1):32-36.
18. Boffard JB, Jung RO, Ch. C. Lin and A. E. Wendt, "Measurement of metastable and resonance level densities in rare-gas plasmas by optical emission spectroscopy", Plasma Sources Sci. Technol. 2009;18(3):1-11.
19. Hebner GA. Spatially resolved, exited state densities and neutral and ion temperatures in inductively coupled plasmas. J. Appl. Phys. 1996;80(5):2624-2636.
20. Leonhardt D, Eddy CR, Shamamian VA, Fensler RF, Butler JE. Argon metastables in a high-density processing plasma", J. Appl. Phys. 1998;83(6):2971-2978.

21. Lotz W. Electron-impact ionization cross-sections for atoms up to Z= 108", Z. Phys. 1970;232: 101.

Biography of author(s)

I. I. Usatov
Bauman Moscow State Technical University, Mytishchi Branch, 141005, Mytischi-5, Moscow Region, Russia.

Igor Usatov graduated from the Moscow Institute of Electronics and Mathematics in 2009. Igor Usatov is Associate Professor at the Department of Higher Mathematics and Physics, Space Faculty, of Bauman Moscow State Technical University (Mytishchi branch). He received Cand. Sci.(Tech.) in Elements and Devices of Computer Technology and Control Systems in 2013. His current research interests include high-power impulse magnetron sputtering discharge, plasma diagnosis, data acquisition and control system.

N. P. Poluektov
Bauman Moscow State Technical University, Mytishchi Branch, 141005, Mytischi-5, Moscow Region, Russia.

Nikolay Poluektov graduated from the Moscow Institute of Physics and Technology in 1971. He is Professor at the Department of Higher Mathematics and Physics, Space Faculty, of BMSTU (Mytishchi branch). He received Cand. Sci.(Phys.-Math.) in Plasma Physics in 1984 and Dr. Sci.(Tech.) in Thermal Physics in 2005. He is the author of over 100 publications. His current research interests include plasma physics, high-power impulse magnetron sputtering discharge and coating process.

Yu P. Tsar'gorodsev
Bauman Moscow State Technical University, Mytishchi Branch, 141005, Mytischi-5, Moscow Region, Russia.

Yuri Tsar'gorodsev graduated from Lomonosov Moscow State University in 1986. He is Associate Professor of BMSTU (Mytishchi branch). He received Cand. Sci.(Tech.) in Thermal Physics in 1996. His current research interests include DC and high-power impulse magnetron sputtering discharge and coating process, plasma diagnosis, data acquisition and control system.

A. G. Evstigneev
Bauman Moscow State Technical University, Mytishchi Branch, 141005, Mytischi-5, Moscow Region, Russia.

Alexey Evstigneev graduated from the Moscow Aviation Institute in 1968. He is an engineer at the Plasma Physics Laboratory in BMSTU.

I. A. Kamyschov
Bauman Moscow State Technical University, Mytishchi Branch, 141005, Mytischi-5, Moscow Region, Russia.

Igor Kamyschov graduated from the Moscow State Forest University in 1987. He is an engineer at the Plasma Physics Laboratory in BMSTU.

DISCLAIMER
This chapter is an extended version of the article published by the same author(s) in the following journal.
Journal of Modern Physics, 3, 1494-1502, 2012.